Report

Current Biology

Cytokinins initiate secondary growth in the *Arabidopsis* root through a set of LBD genes

Graphical abstract

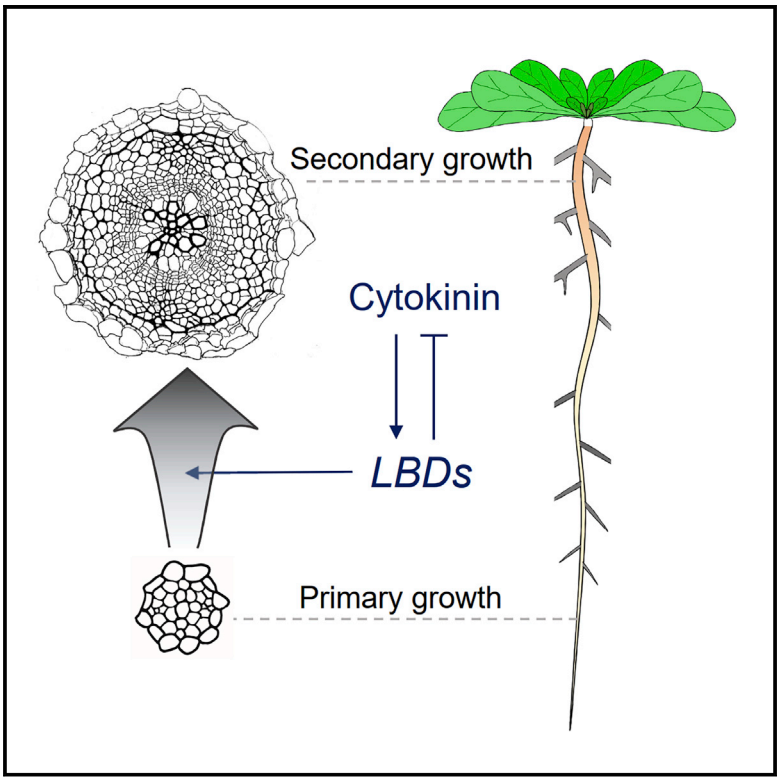

Authors

Lingling Ye, Xin Wang, Munan Lyu, ..., Tiina Blomster, Jing Zhang, Ari Pekka Mähönen

Correspondence

xin.wang@helsinki.fi (X.W.), aripekka.mahonen@helsinki.fi (A.P.M.)

In brief

Ye et al. demonstrate that phytohormone cytokinin and four downstream LATERAL ORGAN BOUNDARIES DOMAIN (LBD) family of transcription factors promote the transition from primary to secondary growth in *Arabidopsis* root. LBDs negatively feed back to cytokinin signaling to keep secondary growth in balance.

Highlights

- Transition from primary to secondary growth occurs gradually in *Arabidopsis* root
- Cytokinins activate secondary growth through a set of LBD genes
- LBDs are required for both cell division and cell growth during secondary growth
- LBDs rapidly inhibit cytokinin signaling

Ye et al., 2021, Current Biology *31*, 3365–3373
August 9, 2021
https://doi.org/10.1016/j.cub.2021.05.036

CellPress

Current Biology

CellPress
OPEN ACCESS

Report

Cytokinins initiate secondary growth in the *Arabidopsis* root through a set of LBD genes

Lingling Ye,[1,2] Xin Wang,[1,2,*] Munan Lyu,[1,2] Riccardo Siligato,[1,2,3] Gugan Eswaran,[1,2] Leo Vainio,[1,2] Tiina Blomster,[1,2] Jing Zhang,[1,2] and Ari Pekka Mähönen[1,2,4,5,*]

[1]Institute of Biotechnology, HiLIFE, University of Helsinki, Helsinki 00014, Finland
[2]Organismal and Evolutionary Biology Research Programme, Faculty of Biological and Environmental Sciences, and Viikki Plant Science Centre, University of Helsinki, Helsinki 00014, Finland
[3]Present address: European Commission, Joint Research Centre, Retieseweg 111, 2440 Geel, Belgium
[4]Twitter: @AP_Mahonen
[5]Lead contact
*Correspondence: xin.wang@helsinki.fi (X.W.), aripekka.mahonen@helsinki.fi (A.P.M.)
https://doi.org/10.1016/j.cub.2021.05.036

SUMMARY

During primary growth, plant tissues increase their length, and as these tissues mature, they initiate secondary growth to increase thickness.[1] It is not known what activates this transition to secondary growth. Cytokinins are key plant hormones regulating vascular development during both primary and secondary growth. During primary growth of *Arabidopsis* roots, cytokinins promote procambial cell proliferation[2,3] and vascular patterning together with the hormone auxin.[4–7] In the absence of cytokinins, secondary growth fails to initiate.[8] Enhanced cytokinin levels, in turn, promote secondary growth.[8,9] Despite the importance of cytokinins, little is known about the downstream signaling events in this process. Here, we show that cytokinins and a few downstream LATERAL ORGAN BOUNDARIES DOMAIN (LBD) family of transcription factors are rate-limiting components in activating and further promoting secondary growth in *Arabidopsis* roots. Cytokinins directly activate transcription of two homologous LBD genes, *LBD3* and *LBD4*. Two other homologous LBDs, *LBD1* and *LBD11*, are induced only after prolonged cytokinin treatment. Our genetic studies revealed a two-stage mechanism downstream of cytokinin signaling: while *LBD3* and *LBD4* regulate activation of secondary growth, *LBD1*, *LBD3*, *LBD4*, and *LBD11* together promote further radial growth and maintenance of cambial stem cells. LBD overexpression promoted rapid cell growth followed by accelerated cell divisions, thus leading to enhanced secondary growth. Finally, we show that LBDs rapidly inhibit cytokinin signaling. Together, our data suggest that the cambium-promoting LBDs negatively feed back into cytokinin signaling to keep root secondary growth in balance.

RESULTS

Recently, we used genome-wide analysis to identify a large set of transcription factors required for normal cambium development.[10] In order to identify which of these factors operate downstream of cytokinin signaling during cambium development, we investigated whether any of their transcriptional regulatory regions are bound by type-B *ARABIDOPSIS* RESPONSE REGULATORS (ARRs),[11–13] the key transcription factors conveying cytokinin signaling (Figure S1A). To further shorten the candidate list, we only considered genes that are also rapidly induced by cytokinins.[14] Using these three criteria, we identified three candidate genes (*SHORT HYPOCOTYL 2*, *LBD3*, and *LBD4*), two of which, *LBD3* and *LBD4*, are close homologs (Figure S1B).[15] We therefore focused on these two genes. First, we tested the response of *LBD3* and *LBD4* to cytokinin by carrying out a qRT-PCR analysis using RNA isolated from *Arabidopsis* roots. *LBD3* and *LBD4* were rapidly induced by cytokinin after just 30 min, a timescale similar to the cytokinin primary response genes *ARR5* and *ARR15* (Figure 1A), confirming previous findings obtained from whole plants.[16] This transcriptional induction also occurred in the presence of the protein synthesis inhibitor cycloheximide (Figure 1B). Furthermore, the basal expression level and cytokinin responsiveness of *LBD3* and *LBD4* were reduced in type-B *ARR* double mutants (Figure S1C). These data together suggest that *LBD3* and *LBD4* are direct targets of type-B ARRs.

Next, we compared the spatial expression of $LBD3_{pro}$*:erYFP* and $LBD4_{pro}$*:erYFP* with the cytokinin response marker $TCSn_{pro}$*:erYFP*[18,19] along the primary root. Each reporter had a graded expression pattern along the root with a maximum in the upper, mature region of root or in the hypocotyl (Figure 1F). There was also a local maximum in the root tip (Figure 1F). Cytokinin treatment rapidly induced the expression of *TCSn*, *LBD3*, and *LBD4* (Figure 1F), and reduction of cytokinin levels by inducible overexpression of the cytokinin degradation enzyme *CYTOKININ*

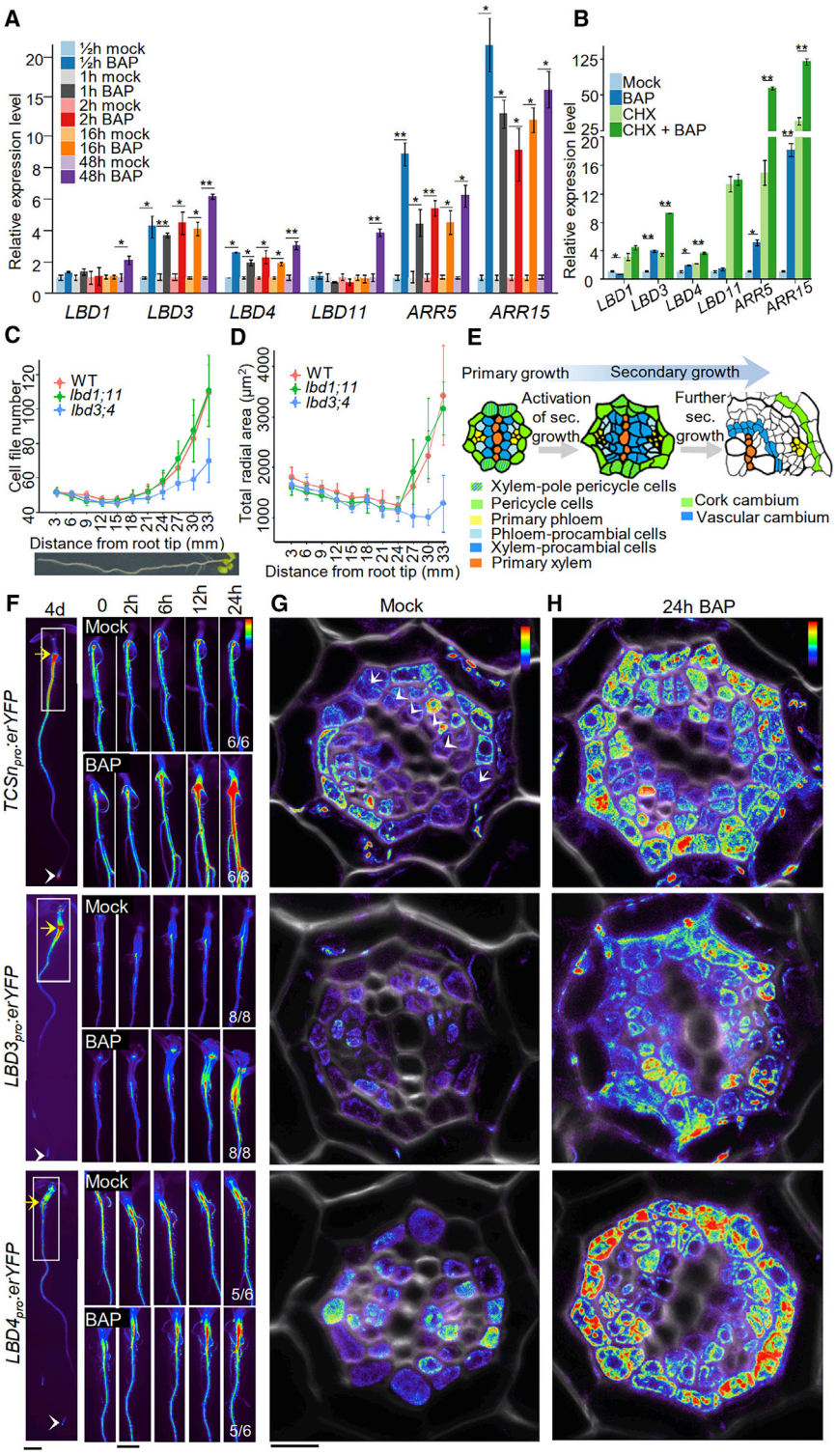

Figure 1. *LBD3* and *LBD4* are cytokinin primary response genes

(A) qRT-PCR analysis of gene transcription after a time course of BAP treatment in 5-day-old roots.

(B) qRT-PCR analysis of gene transcription in 5-day-old plants (whole plants) after mock or BAP treatment in the absence or presence of cycloheximide (CHX).

(C and D) Cell file number (C) and total radial area (D) of pericycle and procambium lineage of 7-day-old roots were quantified (data are presented as mean ± SD, n = 7–31). See Figure S2A for details. Roots were cross-sectioned in 3 mm intervals. x axis indicates the distance of cross-sections from root tip.

(E) Schematic illustration of the developmental progression of root primary vascular tissue into secondary vascular tissue. Adopted from Smetana et al.[17]

(F) Stereo microscopy of fluorescent reporter lines of 4-day-old (left panel) and 6-day-old (right panels) roots. Time course visualization after BAP or mock treatment (right panels). Numbers represent the frequency of the observed expression in independent roots. Yellow arrows indicate the root-hypocotyl junction. White arrowheads mark root tips. White boxes approximately represent the corresponding region visualized in the right panels.

(G and H) Confocal microscopy (heatmap) of $TCSn_{pro}$:*erYFP*, $LBD3_{pro}$:*erYFP* and $LBD4_{pro}$:*erYFP* root cross-sections. 6-day-old plants were treated for 24 h with mock (G) or 1 μM BAP (H). Sections were collected from the region undergoing activation of secondary growth (~1.5 cm below the root-hypocotyl junction). Arrowheads and arrows indicate cell divisions in the procambium and pericycle, respectively (G).

Data are presented as mean ± SE from three biological replicates in (A) and (B). Two-tailed t test. *$p < 0.05$; **$p < 0.01$. Scale bars, 1 mm (F) and 10 μm (G and H). See also Figures S1 and S2A.

OXIDASE 7 (*CKX7*)[20] led to reduced fluorescence of all three reporters (Figure S1D). These data demonstrate that *LBD3* and *LBD4* expression in the root is tightly controlled by cytokinins.

During primary growth, procambial cells within the root apical meristem undergo periclinal cell division (i.e., division along the plane parallel to the root surface) controlled by cytokinin and auxin and a set of downstream transcription factors.[2–7,21,22] These cell divisions terminate as the cells exit the meristem, and thus, the vascular cell file number remains stable until the activation of secondary growth (i.e., radial growth; Figures 1C–1E). During activation, the first divisions in procambium and pericycle cells are sporadic (15~18 mm from root tip), followed by frequent divisions and radial cell growth along the maturing root (Figures 1C, 1D, and S2A), thus leading to secondary growth (~24–27 mm from the root tip; Figure 1D). Pericycle cells and a subset of procambial cells (xylem procambial cells) give rise to two secondary meristems, cork cambium and vascular cambium, respectively. Xylem-pole pericycle cells produce both vascular and cork cambial cells from their circumferential position (Figure 1E).[17] *LBD3* and *LBD4*

CellPress
OPEN ACCESS

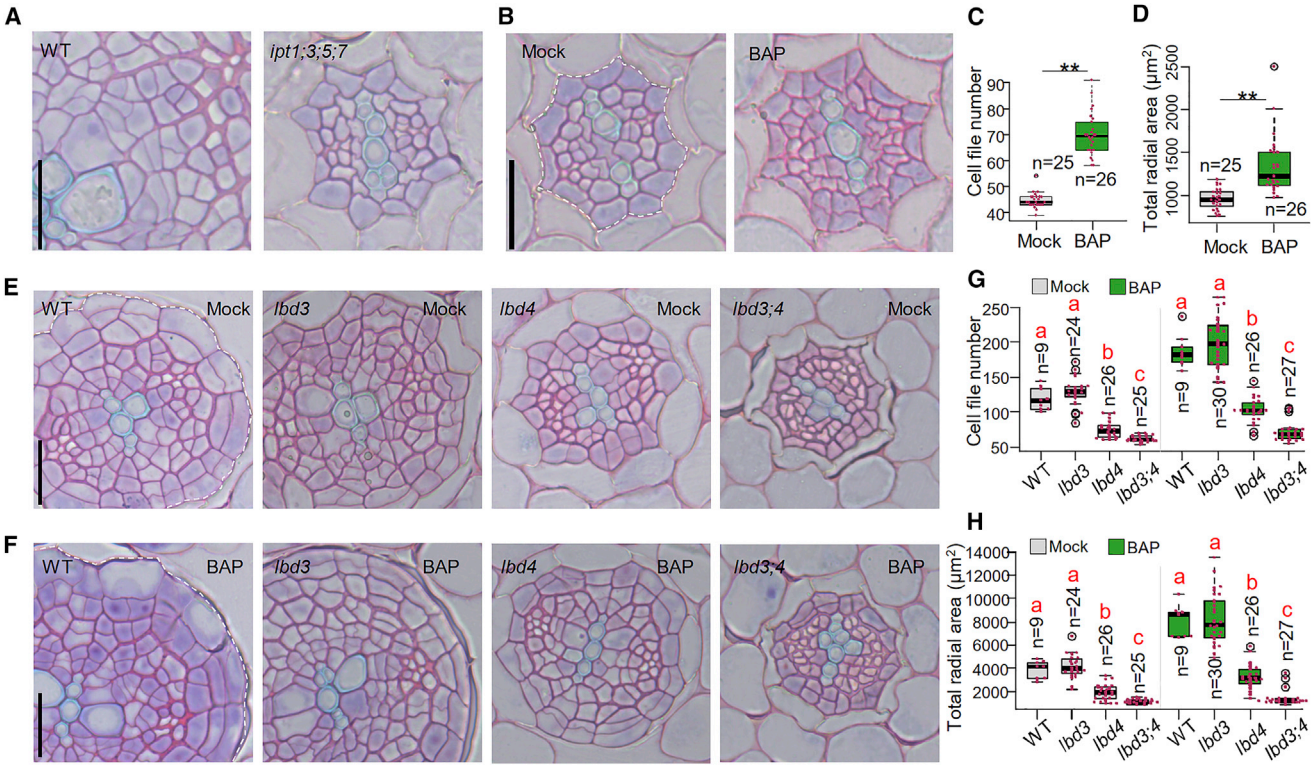

Figure 2. Cytokinin is sufficient to activate cambium prematurely, and this requires *LBD3* and *LBD4*

(A) Cross-sections of 10-day-old wild-type (WT) and *ipt1;3;5;7* roots.

(B) Cross-sections of 5-day-old WT roots. 3-day-old roots were treated for 2 days with mock or 1 μM BAP. Cells and area inside of dotted line were considered in cell file number (C) and total radial area quantifications (D), respectively.

(C and D) Quantification of cell file number (C) and total radial area (D) in the experiment presented in (B). Two-tailed t test. **$p < 0.01$.

(E and F) Cross-sections of WT, *lbd3*, *lbd4*, and *lbd3;4* in 8-day-old roots. Six-day-old roots were treated for 2 days with mock (E) or 1 μM BAP (F). Cells and area inside of dotted line were considered in cell file number (G) and total radial area quantifications (H), respectively.

(G and H) Quantification of cell file number (G) and total radial area (H) in the experiment presented in (E) and (F).

Sections were collected from the main roots 5 mm below the hypocotyl-root junction. Scale bars, 20 μm. Red dots indicate cell numbers or radial area in individual roots (C, D, G, and H). n, number of independent roots analyzed. A separate ANOVA test was performed for mock and BAP treatment. Different red letters indicate significant differences at level alpha = 0.05, as determined by a one-way ANOVA with Tamhane's post-test. The exact p values for each comparison can be found in Data S2A–S2D. See also Figures S3A–S3E and Data S2A–S2D.

are expressed in procambial and pericycle cell lineages during the activation of secondary growth (Figure 1G), and this expression is enhanced in the same cell lineages after cytokinin treatment (Figure 1H). The elevated LBD and *TCS* expression in the mature, upper region of the root (Figure 1F) coincides with the activation of procambial and pericycle cell divisions (Figure 1G). Mutant lacking four genes encoding ATP/ADP ISOPENTENYLTRANSFERASES (IPTs),[23] key enzymes for cytokinin biosynthesis, fails to initiate secondary growth in the root (Figure 2A).[8] Thus, our results raised the hypothesis that the gradual increase of cytokinin signaling as a root matures triggers secondary growth. To test this hypothesis, we transferred 3-day-old seedlings (i.e., before cambium activation) onto cytokinin-containing medium for 2 days. While procambium and pericycle lineages in control seedlings underwent no or only a few cambial cells divisions, cytokinin-treated roots had a number of cell divisions in both lineages, resulting in an increased number of cell files in pericycle and procambial cell lineages (Figures 2B and 2C) and increased radial growth (Figure 2D). These results demonstrate that cytokinins are rate-limiting factors in the activation of secondary growth.

Next, we asked whether *LBD3* and *LBD4* have a role during and after the activation of secondary growth. We generated knockout mutants of both genes via *CRISPR-Cas9*-mediated genome editing (Figure S2B). Before the onset of secondary growth, both single mutants and the *lbd3;lbd4* double mutant had a normal number of pericycle and vascular cell files (Figure S3A). At the initial stages of secondary development (5-day-old roots; 5 mm below the hypocotyl-root junction), the *lbd3;lbd4* double mutant already had significantly fewer cell files than wild type (Figures S3B and S3D). 3 days later (8-day-old roots), *lbd4*, but not *lbd3*, also displayed a reduced number of cell files (Figures 2E and 2G). While 8-day-old wild-type roots had produced several layers of cells from both the vascular and cork cambia, *lbd3;lbd4* roots of the same age had undergone just a few cell divisions. To investigate the cell division and radial growth dynamics during the transition to secondary growth, *lbd3;lbd4* roots were serial sectioned from root tip to hypocotyl. Even though the mutant shows progressively less cell files than wild type, the activation of the first cell divisions appeared not to be delayed (Figures 1C and S2A). However, an

increase in cross-sectional area was observed later in *lbd3;lbd4* (33 mm from root tip) than in wild type (24 mm; Figure 1D), indicating that *LBD3* and *LBD4* are required for activation of secondary growth. These two LBDs seem to mainly operate during secondary growth, because the primary root length and shoot size of the *lbd3;lbd4* double mutant appeared similar to wild type (Figures S3G and S3H). We also tested whether *LBD3* and *LBD4* mediate cytokinin-induced secondary growth. After a 2-day cytokinin treatment, *lbd4* had far fewer additional cell files than wild type, and even fewer were seen in *lbd3;lbd4* (Figures 2E–2G and S3B–S3D). Similar resistance for cytokinin was observed also in radial growth (Figures 2H and S3E). Together, these results indicate that *LBD3* and *LBD4* are major factors acting downstream of cytokinin signaling to activate secondary growth.

To dig deeper into potential redundancy for *LBD3* and *LBD4*, we turned our attention to the closest homologs, *LBD1* and *LBD11* (Figure S1B).[15] Unlike *LBD3* and *LBD4*, *LBD1* and *LBD11* were induced only after prolonged cytokinin treatment, suggesting that they are not primary response genes (Figures 1A, 1B, S1E, and S1F). Similar to $LBD3_{pro}$*:erYFP* and $LBD4_{pro}$*:erYFP*, both $LBD1_{pro}$*:erYFP* and $LBD11_{pro}$*:erYFP* are expressed in the secondary tissue, albeit more weakly (Figure 3A). While $LBD1_{pro}$*:erYFP* is expressed predominantly in the secondary phloem and vascular cambium, expression of $LBD11_{pro}$*:erYFP* is somewhat variable in the secondary xylem, vascular cambium, and periderm (Figure S1G). To investigate whether *LBD1* and *LBD11* have a role in cambium development, we generated knockout mutants through genome editing (Figure S2B). Because the *lbd1;lbd11* double mutant did not have defects during activation of secondary growth (Figures 1C, 1D, 3B, and S2A) and had only a slightly reduced number of cell files in 14-day-old roots (Figure 3H), we combined *lbd3;lbd4* with *lbd1* and *lbd11*. 7-day old *lbd1;lbd3;lbd4*, *lbd1;lbd3;lbd4;lbd11*, and *lbd3;lbd4;lbd11* roots showed a reduction in cell file number similar to *lbd3;lbd4* (Figures 3B and 3C); however, in 14-day-old roots, the triple and quadruple mutants showed a further reduction in cell file number (Figures 3D and 3H). This phenotype was associated with the frequent differentiation of vascular cambium cells located between the primary xylem and the phloem (Figures 3D and 3G), indicating that the LBDs are required for stem cell maintenance. Despite the strong cambial phenotype, shoots of *lbd1;lbd3;lbd4;lbd11* appeared similar to wild type (Figure S3H). Taken together, these results indicate that cytokinin signaling initiates a two-stage process at the onset of secondary growth: *LBD3* and *LBD4* mediate the transition from primary to secondary growth, and this is followed by co-operation between *LBD1*, *LBD3*, *LBD4*, and *LBD11* to promote further secondary growth and cambium stem cell maintenance.

Differentiation of the cambial cells between the primary xylem and the phloem is reminiscent of the phenotype of a double mutant lacking both *PHLOEM INTERCALATED WITH XYLEM/TDIF RECEPTOR* (*PXY/TDR*) and *WUSCHEL-RELATED* HOMEOBOX4 (*WOX4*).[24] We therefore wondered whether *TDR* and *WOX4* operate in the same pathway as the LBDs. To test this, we first analyzed the transcription levels of *TDR* and *WOX4* in 14-day-old *lbd3;lbd4;lbd11* mutant. The transcript level of both appeared unchanged compared with wild type (Figure 3F). Additionally, the *lbd3;lbd4;wox4* mutant displayed frequent cambium cell differentiation adjacent to primary phloem, a phenotype that is not seen in either *lbd3;lbd4* or *wox4* alone (Figures 3E and 3G). The cambium cell differentiation phenotype was more frequent in the *lbd3;lbd4;lbd11;tdr* mutant than in any of the parental mutant combinations and was accompanied by a further reduction of secondary growth (Figures 3E, 3G, and 3H). The additive phenotype indicates redundant roles for the LBDs and *TDR-WOX4* in cambium stem cell maintenance; however, it is unclear whether they operate in the same or parallel pathways.

Because the LBDs encode transcription factors,[25] we examined signaling events downstream of them by generating inducible overexpression lines of each of the four LBDs. We carried out transcript profiling of *LBD3* and *LBD11* lines, thus covering one representative from each subclade (Figure S1B). RNA was isolated from the mature part of the root after an 8-h and 24-h induction, and this was followed by RNA sequencing (RNA-seq) analysis (Data S1A–S1H). Examination of hormone-related genes revealed differential regulation of cytokinin, auxin, and abscisic acid biosynthesis and signaling (Table S2). This is in accordance with the reduced cytokinin, auxin, and abscisic acid levels in *Arabidopsis* shoots when *LBD3* was constitutively overexpressed.[16]

The most striking result was that all of the type-A *ARR*s expressed in the mature root were already downregulated after 8 h of *LBD3* or *LBD11* induction (Figure 4A). Type-A *ARR*s are rapidly transcriptionally upregulated by cytokinins and are thus considered to be the primary cytokinin response genes.[26] qRT-PCR analysis after induction of any of the four LBDs also showed a rapid reduction of *ARR5* and *ARR15* transcript levels, confirming our RNA-seq findings (Figure 4B). In addition, induction of *LBD3* led to reduced fluorescence of $ARR5_{pro}$*:erYFP* and $TCSn_{pro}$*:nYFP* (Figures 4C and 4D). It has been previously shown that constitutive overexpression of *LBD3* reduces cytokinin levels in aerial parts of seedlings,[16] suggesting that *LBD3* inhibits cytokinin signaling by inhibiting cytokinin biosynthesis or promoting its degradation. However, our RNA-seq data revealed that *LBD3* or *LBD11* induction led to downregulation of genes encoding both cytokinin biosynthesis and degradation enzymes as well as signaling components (Table S2). Additionally, $TCSn_{pro}$*:nYFP* downregulation by *LBD3* induction occurred equally rapidly (8 h) with induction of *CKX7* (Figures S4A and S4B). Therefore, the mechanism by which the LBDs inhibit cytokinin signaling appears to be complex and thus remains unresolved. Finally, $TCSn_{pro}$*:nYFP* and $ARR5_{pro}$*:erYFP* fluorescence was enhanced in *lbd3;lbd4* (Figures 4E–4G), and *ARR5* and *ARR15* were significantly elevated in *lbd3;lbd4;lbd11* (Figure 3F). Together, these findings demonstrate that LBD1, LBD3, LBD4, and LBD11 inhibit cytokinin signaling by regulating cytokinin levels and/or signaling.

Because the LBDs regulate cambium development, we compared the list of differentially expressed genes after LBD induction with a list of cambium-enriched genes.[10] Approximately 25% of cambial-enriched genes were already differentially regulated after an 8-h induction of *LBD3* or *LBD11*, and the proportion reached 47% after a 24-h induction of *LBD3*, indicating an intimate link between LBDs and cambium development (Figure S4D; Data S1I). We also conducted a gene ontology (GO) enrichment analysis of the *LBD3* and *LBD11* transcript profiling data. Several categories were over-represented, but processes associated with primary cell wall modification, such as "pectin

CellPress
OPEN ACCESS

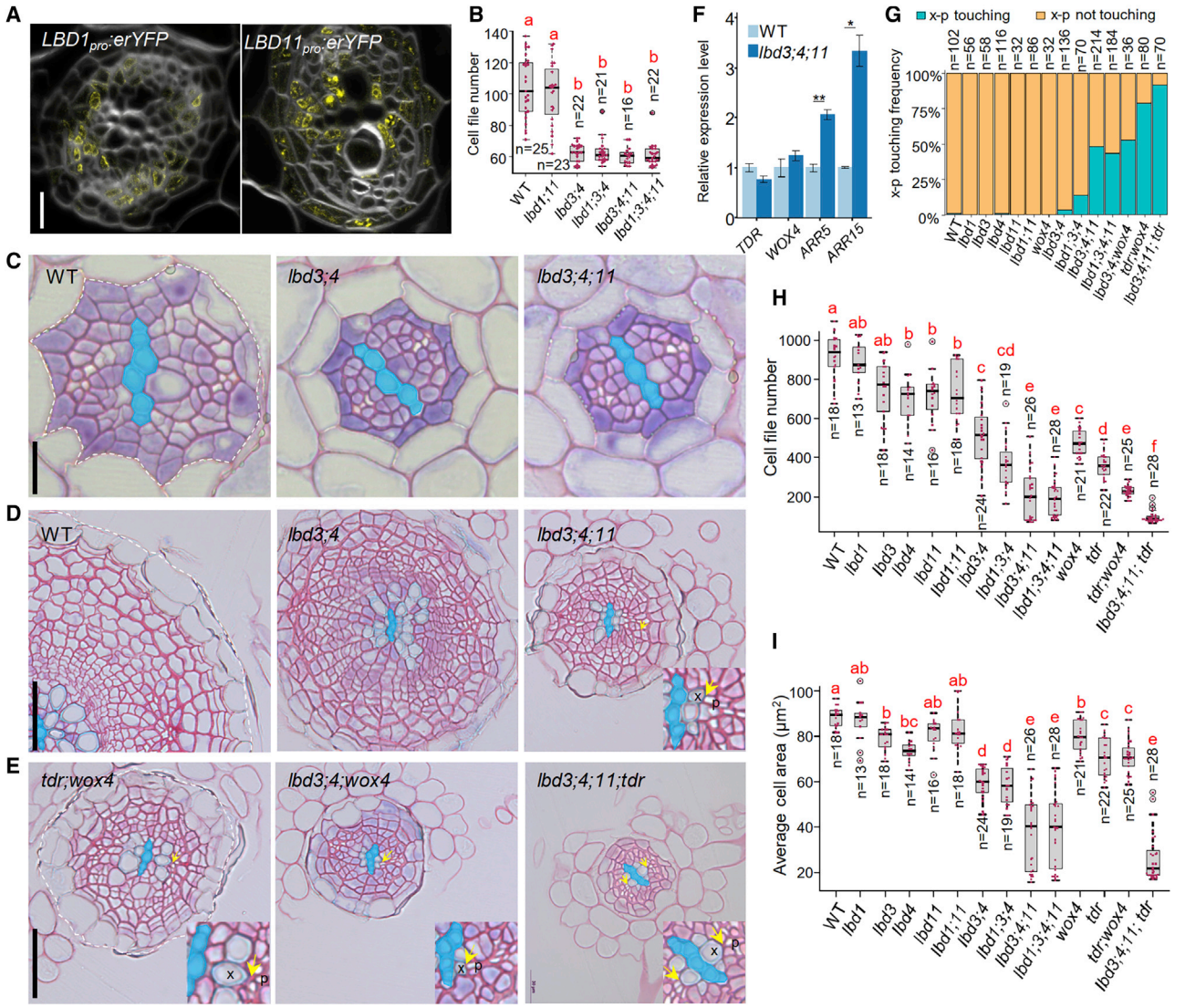

Figure 3. LBDs redundantly promote cambium stem cell maintenance together with *TDR* and *WOX4*

(A) Confocal microscopy of *LBD1*$_{pro}$*:erYFP* and *LBD11*$_{pro}$*:erYFP* root cross-sections. Sections were collected from 5 mm below the root-hypocotyl junction of 7-day-old roots.

(B) Quantification of cell file number in pericycle and procambium lineage. Seven-day-old roots are shown.

(C) Root cross-sections in 7-day-old roots. Cells inside of dotted line were considered in cell file number quantifications (B).

(D and E) Root cross-sections in 14-day-old roots. p, phloem cell (i.e., white sieve element cell); x, xylem vessel. Arrows mark xylem vessels adjacent to phloem cells, indicating that vascular cambium cells have been differentiated in this position, which is not observed in WT. Cells inside of dotted line were considered in cell file number quantifications (H) and in average cell area calculations (I).

(F) qRT-PCR analysis of gene transcription in WT and the *lbd3;4;11* triple mutant. RNA was extracted from the upper 1 cm part of the main root just below the root-hypocotyl junction in 14-day-old plants. Data are presented as mean ± SE from three biological replicates. Two-tailed t test. *$p < 0.05$; **$p < 0.01$.

(G) Frequency of observed phloem adjacent to the xylem (x-p touching) phenotype in WT and in mutants. n, total number of events analyzed.

(H and I) Quantification of root cell file number (H) and average radial cell area (I) in 14-day-old WT and mutants.

Primary xylem cells (i.e., xylem axis) are false colored in blue (C–E). Red dots indicate cell file number or average cell area in individual roots (B, H, and I). n, number of independent roots analyzed. Different red letters indicate significant differences at level alpha = 0.05, as determined by one-way ANOVA with Tamhane's post-test. The exact p values for each comparison can be found in Data S2E–S2I. Scale bars, 10 μm (A), 25 μm (C), and 50 μm (D and E). See also Figures S3G and S3H and Data S2E–S2I.

catabolic process'' and ''plant-type cell wall modification,'' were the most notable (Figures S4E and S4F). These data suggest that the LBDs regulate primary cell wall composition and thus may regulate cell wall extensibility.[27] Indeed, 2 days after *LBD1*, *LBD3*, or *LBD11* induction, we observed rapid procambial and pericycle cell growth (Figures 4H and S4G–S4I). When LBDs were induced after cambium activation, enhanced cell growth was associated with more cell divisions and thus accelerated secondary growth (Figures 4I and S4J–S4L). Furthermore, in addition to having fewer cell files, *lbd* mutants also have a

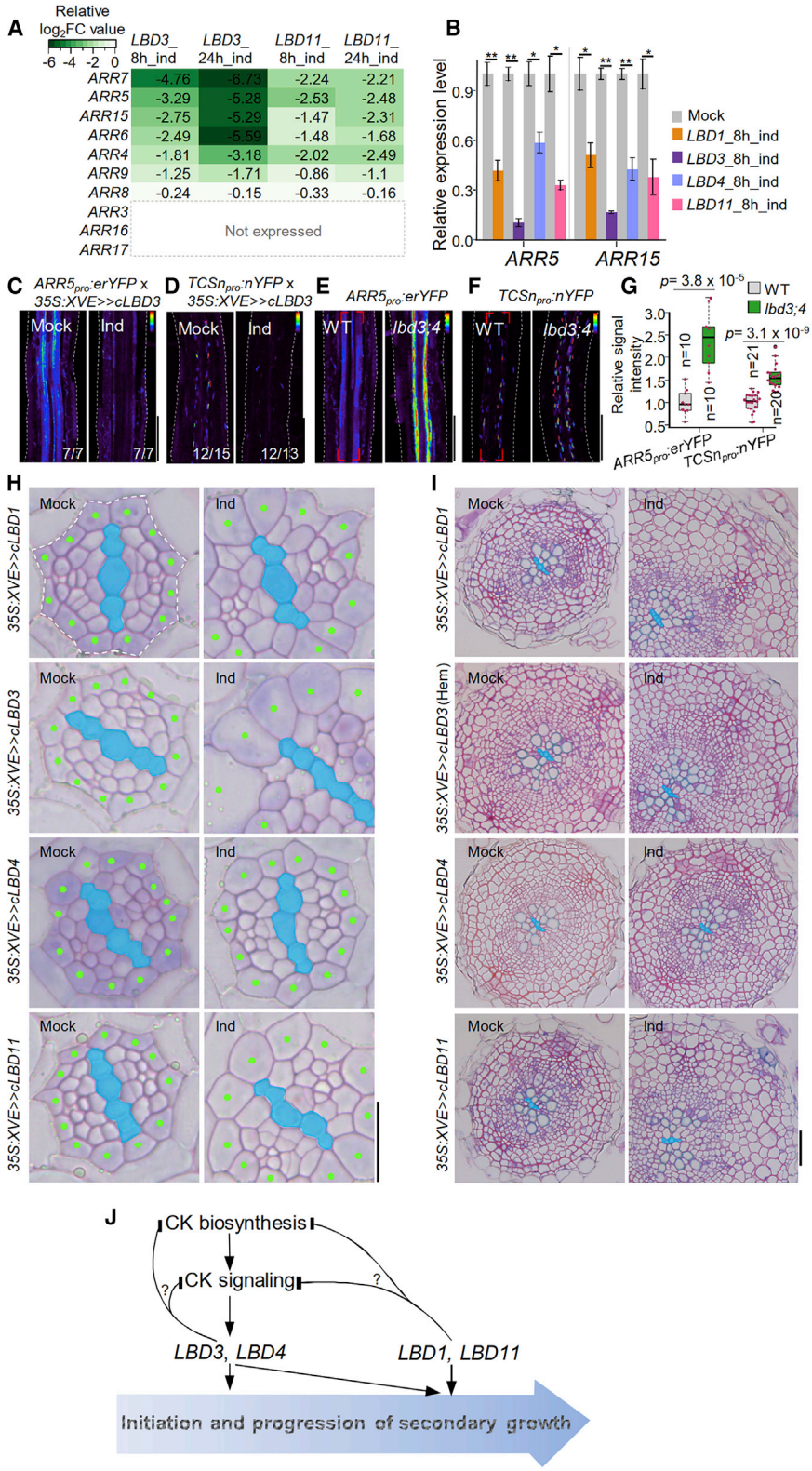

Figure 4. LBDs negatively regulate cytokinin signaling and promote cell growth during secondary growth

(A) Heatmap showing normalized log_2FoldChange (FC) of A-type *ARR*s mRNA in *LBD3* or *LBD11* inducible overexpression RNA-seq data. We considered a gene "not expressed" in mature root if read counts were less than 10.

(B) qRT-PCR analysis of A-type *ARR* (*ARR5* and *ARR15*) transcription in 9-day-old roots (0.5–2 cm below the root-hypocotyl junction, undergoing secondary growth) with 8 h mock or induction. Data are presented as mean ± SE from three biological replicates. Two-tailed t test. *$p < 0.05$; **$p < 0.01$.

(C and D) Confocal microscopy of $ARR5_{pro}$*:erYFP* (C) and $TCSn_{pro}$*:nYFP* (D) after 1-day *LBD3* induction in 6-day-old roots. $ARR5_{pro}$*:erYFP* was analyzed in F1 generation.

(E and F) Confocal microscopy of $ARR5_{pro}$*:erYFP* (E) and $TCSn_{pro}$*:nYFP* (F) in 7-day-old WT and *lbd3;4* roots.

(G) Quantification of average fluorescent signal intensity in (E) and (F). Area marked with brackets (E and F) was quantified. Red dots indicate average fluorescent signal intensity in individual roots. n, number of independent roots analyzed.

(H) Cross-sections of 5-day-old roots of LBD inducible overexpression lines. Three-day-old roots were treated for 2 days with mock or 5 μM 17-β, except in the case of *LBD3*, which was treated with 0.5 μM 17-β. Green dots represent pericycle cells. Cells inside of dotted line were used for cell file quantification in Figure S4G.

(I) Cross-sections of 14-day-old roots of LBD inducible overexpression lines. Eight-day-old roots were treated for 6 days with mock or 5 μM 17-β. Note that 0.5 μM 17-β was used for the *LBD3* hemizygous (hem) line due to dose-dependent effect (Figure S4M).

(J) A model presenting the roles of LBDs during the progression of root secondary growth (large blue arrow) downstream of cytokinin (CK).

Dashed lines represent root boundaries (C–F). Primary xylem cells (i.e., xylem axis) are false colored in blue (H and I). Scale bars, 100 μm (C–F), 20 μm (H), and 50 μm (I). See also Figures S1G and S4, Table S2, and Data S1 and S3.

reduced average cell size in radial dimension (Figure 3I). While also *tdr;wox4* show reduced number of cell files, this phenotype is not associated with markedly reduced average cell size as observed in *lbd3;lbd4;lbd11* (Figure 3I). These data suggest that the LBD proteins promote secondary growth at least in part through promoting controlled cell growth.

DISCUSSION

Previous studies have shown that *LBD3* and *LBD4* are positive regulators of secondary growth in *Arabidopsis*.[10,28] Here, we show that *LBD3* and *LBD4* act redundantly directly downstream of cytokinin signaling to activate secondary growth in the *Arabidopsis* root. Later in development, *LBD1* and *LBD11* also act to promote further secondary growth. These four LBDs are also required to keep cambial stem cells undifferentiated, and they are able to rapidly inhibit cytokinin signaling. These findings allowed us to generate a model (Figure 4J) in which elevated cytokinin signaling in the mature root leads to two stages of LBD expression to first initiate and then maintain secondary growth. The exact role of the negative feedback of LBD expression on cytokinin levels or signaling remains unclear, as does the mechanism by which it is mediated; however, it may serve to maintain stable and responsive signaling, as has been suggested for other genetic networks with negative feedback.[29]

Tissue growth is a result of delicate coordination of cell growth and cell division. Loss of LBDs leads to a reduced number of cell files and reduced radial cell size, thus resulting in diminished secondary growth. However, induction of LBDs promotes rapid cell growth, and accelerated cell divisions appear only after a longer induction. It is possible that LBDs require co-operation with other factors to promote cell division. Alternatively, there could be other factors downstream of cytokinin that promote cell divisions, while LBDs are in charge of promoting cell growth. Such factors could be the PEAR genes[21] or *Dof2.1*,[22] which has been shown to promote periclinal cell divisions downstream of cytokinin in root primary vascular tissue.

Loss of *LBD1*, *LBD3*, *LBD4*, and *LBD11* led to differentiation of cambium cells adjacent to phloem, a phenotype similar to loss of both *TDR* and *WOX4*.[24] Our genetic analysis did not determine whether the LBDs and *TDR-WOX4* operate in the same pathway or parallel pathways to maintain cambial stem cells. In support of the idea that they function in the same pathway, it has also been shown that *LBD4* operates downstream of auxin and *TDR* signaling,[28] and both *WOX4* and *TDR* are regulated by auxin.[17,30] LBDs seem to broadly regulate the transcription of genes encoding signaling components or metabolic enzymes for several plant hormones (Table S2). Thus, the interaction of the LBDs with *TDR-WOX4* and hormonal pathways appears complex and warrants further investigation.

Cytokinins are also critical players in secondary growth in poplar trees.[31,32] Additionally, overexpression of the poplar homolog of *LBD1* or its dominant-negative version has been shown to lead to enhanced or decreased secondary growth in poplar stems, respectively.[33] It remains to be determined whether this and the other related LBDs regulate cambial development in tree stems by promoting cell growth and whether there is a negative feedback mechanism with cytokinin signaling similar to in *Arabidopsis*.

STAR★METHODS

Detailed methods are provided in the online version of this paper and include the following:

- KEY RESOURCES TABLE
- RESOURCE AVAILABILITY
  - Lead contact
  - Materials availability
  - Data and code availability
- EXPERIMENTAL MODEL AND SUBJECT DETAILS
- METHOD DETAILS
  - Plant material and growth conditions
  - Molecular cloning and transformation
  - Mutant generation by CRISPR/Cas9
  - Microscopy and image processing
  - qRT-PCR
  - RNA-Seq
- QUANTIFICATION AND STATISTICAL ANALYSIS

SUPPLEMENTAL INFORMATION

Supplemental information can be found online at https://doi.org/10.1016/j.cub.2021.05.036.

ACKNOWLEDGMENTS

We thank A. Vatén and H. Fukuda for sharing published materials; lab members, Y. Helariutta, and A. Bishopp for helpful comments on the manuscript; M. Herpola and M. Iida for technical assistance; B. Wybouw for help on statistical analysis; Biodata Analytics Unit, Light Microscopy Unit, and Sequencing and Genomics Laboratory at Institute of Biotechnology; CSC–IT Center for Science, Finland, for computational resources; and S. el-Showk for proofreading of this manuscript. This work was supported by the Academy of Finland (grants no. 316544, no. 266431, no. 304806, and no. 307335), European Research Council (ERC-CoG CORKtheCAMBIA, agreement 819422), and University of Helsinki HiLIFE fellowship. X.W. is also supported by a grant from the Chinese Scholarship Council (CSC). The ORCID IDs for this article are as follows: 0000-0003-3834-862X (L.Y.); 0000-0002-8982-9848 (X.W.); 0000-0003-1645-3488 (M.L.); 0000-0002-1310-2757 (R.S.); 0000-0002-3439-3696 (G.E.); 0000-0001-7113-1604 (T.B.); 0000-0003-4463-7516 (J.Z.); and 0000-0001-6051-866X (A.P.M.).

AUTHOR CONTRIBUTIONS

L.Y., X.W., and A.P.M. designed the experiments. L.Y. conducted most experiments together with X.W. M.L. performed qRT-PCR. R.S. made the initial discovery on cytokinin response gradient and cytokinin activating cambium prematurely. R.S., T.B., and M.L. generated and analyzed CKX7 inducible overexpression lines. L.Y., X.W., G.E., and L.V. quantified cell file number in cross-sections. Earlier findings by J.Z. and T.B. directed our interest toward the LBD genes. T.B. and L.Y. performed RNA-seq data analysis. L.Y., X.W., and A.P.M. analyzed the results and wrote the manuscript, with input from all co-authors.

DECLARATION OF INTERESTS

The authors declare no competing interests.

Received: December 15, 2020
Revised: March 24, 2021
Accepted: May 7, 2021
Published: June 14, 2021

REFERENCES

1. Evert, R.F. (2006). Esau's Plant Anatomy: Meristems, Cells, and Tissues of the Plant Body: Their Structure, Function, and Development, Third Edition (John Wiley & Sons).
2. Mähönen, A.P., Bishopp, A., Higuchi, M., Nieminen, K.M., Kinoshita, K., Törmäkangas, K., Ikeda, Y., Oka, A., Kakimoto, T., and Helariutta, Y. (2006). Cytokinin signaling and its inhibitor AHP6 regulate cell fate during vascular development. Science *311*, 94–98.
3. Mähönen, A.P., Bonke, M., Kauppinen, L., Riikonen, M., Benfey, P.N., and Helariutta, Y. (2000). A novel two-component hybrid molecule regulates vascular morphogenesis of the Arabidopsis root. Genes Dev. *14*, 2938–2943.
4. Bishopp, A., Lehesranta, S., Vatén, A., Help, H., El-Showk, S., Scheres, B., Helariutta, K., Mähönen, A.P., Sakakibara, H., and Helariutta, Y. (2011). Phloem-transported cytokinin regulates polar auxin transport and maintains vascular pattern in the root meristem. Curr. Biol. *21*, 927–932.
5. De Rybel, B., Adibi, M., Breda, A.S., Wendrich, J.R., Smit, M.E., Novák, O., Yamaguchi, N., Yoshida, S., Van Isterdael, G., Palovaara, J., et al. (2014). Plant development. Integration of growth and patterning during vascular tissue formation in Arabidopsis. Science *345*, 1255215.
6. el-Showk, S., Help-Rinta-Rahko, H., Blomster, T., Siligato, R., Marée, A.F., Mähönen, A.P., and Grieneisen, V.A. (2015). Parsimonious model of vascular patterning links transverse hormone fluxes to lateral root initiation: auxin leads the way, while cytokinin levels out. PLoS Comput. Biol. *11*, e1004450.
7. Muraro, D., Mellor, N., Pound, M.P., Help, H., Lucas, M., Chopard, J., Byrne, H.M., Godin, C., Hodgman, T.C., King, J.R., et al. (2014). Integration of hormonal signaling networks and mobile microRNAs is required for vascular patterning in Arabidopsis roots. Proc. Natl. Acad. Sci. USA *111*, 857–862.
8. Matsumoto-Kitano, M., Kusumoto, T., Tarkowski, P., Kinoshita-Tsujimura, K., Václavíková, K., Miyawaki, K., and Kakimoto, T. (2008). Cytokinins are central regulators of cambial activity. Proc. Natl. Acad. Sci. USA *105*, 20027–20031.
9. Randall, R.S., Miyashima, S., Blomster, T., Zhang, J., Elo, A., Karlberg, A., Immanen, J., Nieminen, K., Lee, J.Y., Kakimoto, T., et al. (2015). AINTEGUMENTA and the D-type cyclin CYCD3;1 regulate root secondary growth and respond to cytokinins. Biol. Open *4*, 1229–1236.
10. Zhang, J., Eswaran, G., Alonso-Serra, J., Kucukoglu, M., Xiang, J., Yang, W., Elo, A., Nieminen, K., Damén, T., Joung, J.G., et al. (2019). Transcriptional regulatory framework for vascular cambium development in Arabidopsis roots. Nat. Plants *5*, 1033–1042.
11. Potter, K.C., Wang, J., Schaller, G.E., and Kieber, J.J. (2018). Cytokinin modulates context-dependent chromatin accessibility through the type-B response regulators. Nat. Plants *4*, 1102–1111.
12. Xie, M., Chen, H., Huang, L., O'Neil, R.C., Shokhirev, M.N., and Ecker, J.R. (2018). A B-ARR-mediated cytokinin transcriptional network directs hormone cross-regulation and shoot development. Nat. Commun. *9*, 1604.
13. Zubo, Y.O., Blakley, I.C., Yamburenko, M.V., Worthen, J.M., Street, I.H., Franco-Zorrilla, J.M., Zhang, W., Hill, K., Raines, T., Solano, R., et al. (2017). Cytokinin induces genome-wide binding of the type-B response regulator ARR10 to regulate growth and development in *Arabidopsis*. Proc. Natl. Acad. Sci. USA *114*, E5995–E6004.
14. Bhargava, A., Clabaugh, I., To, J.P., Maxwell, B.B., Chiang, Y.H., Schaller, G.E., Loraine, A., and Kieber, J.J. (2013). Identification of cytokinin-responsive genes using microarray meta-analysis and RNA-Seq in Arabidopsis. Plant Physiol. *162*, 272–294.
15. Iwakawa, H., Ueno, Y., Semiarti, E., Onouchi, H., Kojima, S., Tsukaya, H., Hasebe, M., Soma, T., Ikezaki, M., Machida, C., and Machida, Y. (2002). The ASYMMETRIC LEAVES2 gene of Arabidopsis thaliana, required for formation of a symmetric flat leaf lamina, encodes a member of a novel family of proteins characterized by cysteine repeats and a leucine zipper. Plant Cell Physiol. *43*, 467–478.
16. Naito, T., Yamashino, T., Kiba, T., Koizumi, N., Kojima, M., Sakakibara, H., and Mizuno, T. (2007). A link between cytokinin and ASL9 (ASYMMETRIC LEAVES 2 LIKE 9) that belongs to the AS2/LOB (LATERAL ORGAN BOUNDARIES) family genes in *Arabidopsis thaliana*. Biosci. Biotechnol. Biochem. *71*, 1269–1278.
17. Smetana, O., Mäkilä, R., Lyu, M., Amiryousefi, A., Sánchez Rodríguez, F., Wu, M.F., Solé-Gil, A., Leal Gavarrón, M., Siligato, R., Miyashima, S., et al. (2019). High levels of auxin signalling define the stem-cell organizer of the vascular cambium. Nature *565*, 485–489.
18. Vatén, A., Soyars, C.L., Tarr, P.T., Nimchuk, Z.L., and Bergmann, D.C. (2018). Modulation of asymmetric division diversity through cytokinin and SPEECHLESS regulatory interactions in the Arabidopsis stomatal lineage. Dev. Cell *47*, 53–66.e5.
19. Zürcher, E., Tavor-Deslex, D., Lituiev, D., Enkerli, K., Tarr, P.T., and Müller, B. (2013). A robust and sensitive synthetic sensor to monitor the transcriptional output of the cytokinin signaling network in planta. Plant Physiol. *161*, 1066–1075.
20. Köllmer, I., Novák, O., Strnad, M., Schmülling, T., and Werner, T. (2014). Overexpression of the cytosolic cytokinin oxidase/dehydrogenase (CKX7) from Arabidopsis causes specific changes in root growth and xylem differentiation. Plant J. *78*, 359–371.
21. Miyashima, S., Roszak, P., Sevilem, I., Toyokura, K., Blob, B., Heo, J.O., Mellor, N., Help-Rinta-Rahko, H., Otero, S., Smet, W., et al. (2019). Mobile PEAR transcription factors integrate positional cues to prime cambial growth. Nature *565*, 490–494.
22. Smet, W., Sevilem, I., de Luis Balaguer, M.A., Wybouw, B., Mor, E., Miyashima, S., Blob, B., Roszak, P., Jacobs, T.B., Boekschoten, M., et al. (2019). DOF2.1 controls cytokinin-dependent vascular cell proliferation downstream of TMO5/LHW. Curr. Biol. *29*, 520–529.e6.
23. Miyawaki, K., Tarkowski, P., Matsumoto-Kitano, M., Kato, T., Sato, S., Tarkowska, D., Tabata, S., Sandberg, G., and Kakimoto, T. (2006). Roles of Arabidopsis ATP/ADP isopentenyltransferases and tRNA isopentenyltransferases in cytokinin biosynthesis. Proc. Natl. Acad. Sci. USA *103*, 16598–16603.
24. Hirakawa, Y., Kondo, Y., and Fukuda, H. (2010). TDIF peptide signaling regulates vascular stem cell proliferation via the WOX4 homeobox gene in Arabidopsis. Plant Cell *22*, 2618–2629.
25. Husbands, A., Bell, E.M., Shuai, B., Smith, H.M.S., and Springer, P.S. (2007). LATERAL ORGAN BOUNDARIES defines a new family of DNA-binding transcription factors and can interact with specific bHLH proteins. Nucleic Acids Res. *35*, 6663–6671.
26. To, J.P., and Kieber, J.J. (2008). Cytokinin signaling: two-components and more. Trends Plant Sci. *13*, 85–92.
27. Cosgrove, D.J. (2016). Plant cell wall extensibility: connecting plant cell growth with cell wall structure, mechanics, and the action of wall-modifying enzymes. J. Exp. Bot. *67*, 463–476.
28. Smit, M.E., McGregor, S.R., Sun, H., Gough, C., Bågman, A.M., Soyars, C.L., Kroon, J.T., Gaudinier, A., Williams, C.J., Yang, X., et al. (2020). A PXY-mediated transcriptional network integrates signaling mechanisms to control vascular development in Arabidopsis. Plant Cell *32*, 319–335.
29. Alon, U. (2006). An Introduction to Systems Biology: Design Principles of Biological Circuits (CRC).
30. Brackmann, K., Qi, J., Gebert, M., Jouannet, V., Schlamp, T., Grünwald, K., Wallner, E.S., Novikova, D.D., Levitsky, V.G., Agustí, J., et al. (2018). Spatial specificity of auxin responses coordinates wood formation. Nat. Commun. *9*, 875.
31. Immanen, J., Nieminen, K., Smolander, O.P., Kojima, M., Alonso Serra, J., Koskinen, P., Zhang, J., Elo, A., Mähönen, A.P., Street, N., et al. (2016). Cytokinin and auxin display distinct but interconnected distribution and signaling profiles to stimulate cambial activity. Curr. Biol. *26*, 1990–1997.
32. Nieminen, K., Immanen, J., Laxell, M., Kauppinen, L., Tarkowski, P., Dolezal, K., Tähtiharju, S., Elo, A., Decourteix, M., Ljung, K., et al. (2008). Cytokinin signaling regulates cambial development in poplar. Proc. Natl. Acad. Sci. USA *105*, 20032–20037.

33. Yordanov, Y.S., Regan, S., and Busov, V. (2010). Members of the LATERAL ORGAN BOUNDARIES DOMAIN transcription factor family are involved in the regulation of secondary growth in Populus. Plant Cell *22*, 3662–3677.

34. Koncz, C., and Schell, J. (1986). The promoter of T_L-DNA gene *5* controls the tissue-specific expression of chimaeric genes carried by a novel type of *Agrobacterium* binary vector. Mol. Gen. Genet. *204*, 383–396.

35. Murashige, T., and Skoog, F. (1962). A revised medium for rapid growth and bio assays with tobacco tissue cultures. Physiol. Plant. *15*, 473–497.

36. Siligato, R., Wang, X., Yadav, S.R., Lehesranta, S., Ma, G., Ursache, R., Sevilem, I., Zhang, J., Gorte, M., Prasad, K., et al. (2016). MultiSite gateway-compatible cell type-specific gene-inducible system for plants. Plant Physiol. *170*, 627–641.

37. Argyros, R.D., Mathews, D.E., Chiang, Y.H., Palmer, C.M., Thibault, D.M., Etheridge, N., Argyros, D.A., Mason, M.G., Kieber, J.J., and Schaller, G.E. (2008). Type B response regulators of Arabidopsis play key roles in cytokinin signaling and plant development. Plant Cell *20*, 2102–2116.

38. Wang, Z.P., Xing, H.L., Dong, L., Zhang, H.Y., Han, C.Y., Wang, X.C., and Chen, Q.J. (2015). Egg cell-specific promoter-controlled CRISPR/Cas9 efficiently generates homozygous mutants for multiple target genes in Arabidopsis in a single generation. Genome Biol. *16*, 144.

39. Wang, X., Ye, L., Lyu, M., Ursache, R., Löytynoja, A., and Mähönen, A.P. (2020). An inducible genome editing system for plants. Nat. Plants *6*, 766–772.

40. Kallio, M.A., Tuimala, J.T., Hupponen, T., Klemelä, P., Gentile, M., Scheinin, I., Koski, M., Käki, J., and Korpelainen, E.I. (2011). Chipster: user-friendly analysis software for microarray and other high-throughput data. BMC Genomics *12*, 507.

41. Larkin, M.A., Blackshields, G., Brown, N.P., Chenna, R., McGettigan, P.A., McWilliam, H., Valentin, F., Wallace, I.M., Wilm, A., Lopez, R., et al. (2007). Clustal W and Clustal X version 2.0. Bioinformatics *23*, 2947–2948.

42. Yu, G., Wang, L.G., Han, Y., and He, Q.Y. (2012). clusterProfiler: an R package for comparing biological themes among gene clusters. OMICS *16*, 284–287.

43. Neff, M.M., Turk, E., and Kalishman, M. (2002). Web-based primer design for single nucleotide polymorphism analysis. Trends Genet. *18*, 613–615.

44. Love, M.I., Huber, W., and Anders, S. (2014). Moderated estimation of fold change and dispersion for RNA-seq data with DESeq2. Genome Biol. *15*, 550.

45. Andrews, S. (2010). FastQC: a quality control tool for high throughput sequence data. https://www.bioinformatics.babraham.ac.uk/projects/fastqc/.

46. Schindelin, J., Arganda-Carreras, I., Frise, E., Kaynig, V., Longair, M., Pietzsch, T., Preibisch, S., Rueden, C., Saalfeld, S., Schmid, B., et al. (2012). Fiji: an open-source platform for biological-image analysis. Nat. Methods *9*, 676–682.

47. Wickham, H. (2016). ggplot2: Elegant Graphics for Data Analysis (Springer-Verlag).

48. Warnes, G.R., Bolker, B., Bonebakker, L., Gentleman, R., Huber, W., Liaw, A., Lumley, T., Maechler, M., Magnusson, A., Moeller, S., et al. (2016). Package 'gplots'. Various R programming tools for plotting data. https://cran.r-project.org/web/packages/gplots/gplots.pdf.

49. Anders, S., Pyl, P.T., and Huber, W. (2015). HTSeq–a Python framework to work with high-throughput sequencing data. Bioinformatics *31*, 166–169.

50. Kumar, S., Stecher, G., and Tamura, K. (2016). MEGA7: molecular evolutionary genetics analysis version 7.0 for bigger datasets. Mol. Biol. Evol. *33*, 1870–1874.

51. The R Development Core Team (2013). R: A language and environment for statistical computing (R Foundation for Statistical Computing).

52. Racine, J.S. (2012). RStudio: a platform-independent IDE for R and Sweave. J. Appl. Econ. *27*, 167–172.

53. Kim, D., Pertea, G., Trapnell, C., Pimentel, H., Kelley, R., and Salzberg, S.L. (2013). TopHat2: accurate alignment of transcriptomes in the presence of insertions, deletions and gene fusions. Genome Biol. *14*, R36.

54. Oliveros, J. (2016). Venny. An interactive tool for comparing lists with Venn's diagrams. 2007–2015. https://bioinfogp.cnb.csic.es/tools/venny/index.html.

55. Karimi, M., Inzé, D., and Depicker, A. (2002). GATEWAY vectors for *Agrobacterium*-mediated plant transformation. Trends Plant Sci. *7*, 193–195.

56. Clough, S.J., and Bent, A.F. (1998). Floral dip: a simplified method for *Agrobacterium*-mediated transformation of *Arabidopsis thaliana*. Plant J. *16*, 735–743.

57. Ma, X., Zhang, Q., Zhu, Q., Liu, W., Chen, Y., Qiu, R., Wang, B., Yang, Z., Li, H., Lin, Y., et al. (2015). A robust CRISPR/Cas9 system for convenient, high-efficiency multiplex genome editing in monocot and dicot plants. Mol. Plant *8*, 1274–1284.

58. Kareem, A., Radhakrishnan, D., Wang, X., Bagavathiappan, S., Trivedi, Z.B., Sugimoto, K., Xu, J., Mähönen, A.P., and Prasad, K. (2016). Protocol: a method to study the direct reprogramming of lateral root primordia to fertile shoots. Plant Methods *12*, 27.

59. Ursache, R., Andersen, T.G., Marhavý, P., and Geldner, N. (2018). A protocol for combining fluorescent proteins with histological stains for diverse cell wall components. Plant J. *93*, 399–412.

60. Livak, K.J., and Schmittgen, T.D. (2001). Analysis of relative gene expression data using real-time quantitative PCR and the 2(-Delta Delta C(T)) method. Methods *25*, 402–408.

61. Kanehisa, M., and Goto, S. (2000). KEGG: kyoto encyclopedia of genes and genomes. Nucleic Acids Res. *28*, 27–30.

STAR★METHODS

KEY RESOURCES TABLE

REAGENT or RESOURCE	SOURCE	IDENTIFIER
Bacterial and virus strains		
Agrobacterium tumefaciens c58 GV3101 pMP90	Koncz and Schell[34]	N/A
Escherichia coli DH5α	N/A	N/A
Chemicals, peptides, and recombinant proteins		
17-β-oestradiol (17-β)	Sigma-Aldrich	Cat# 3301
6-benzylaminopurine (BAP)	Sigma-Aldrich	Cat# B3408
Cycloheximide (CHX)	Sigma-Aldrich	Cat#C7698
DdeI (HpyF3I)	ThermoFisher	Cat# FD1884
Dimethyl Sulfoxide (DMSO)	Sigma-Aldrich	Cat# D8418
DL-Phosphinothricin (PPT)	Duchefa Biochemie	Cat# P0159.1000
Dream Taq DNA Polymerase	ThermoFisher	Cat# EP0713
DNase I	ThermoFisher	Cat# EN0521
FTA Classic Card	Sigma-Aldrich	Cat# WHAWB120206
Gateway LR Clonase II Plus enzyme	ThermoFisher	Cat# 12538120
Hygromycin B Gold	InvivoGen	Cat# ant-hg-1
Maxima H Minus Reverse Transcriptase	ThermoFisher	Cat# EP0752
Murashige & Skoog medium	Murashige and Skoog[35] and Duchefa Biochemie	Cat# M 0222.0050
NotI	ThermoFisher	Cat# FD0595
Oligo(dT)18 Primer	ThermoFisher	Cat# SO132
Phusion High-Fidelity DNA Polymerase	ThermoFisher	Cat# F530L
RiboLock RNase Inhibitor	ThermoFisher	Cat# EO0382
Rifampicin	Duchefa Biochemie	Cat# R0146
Ruthenium red	Fluka	Cat# 84071
ScaI	ThermoFisher	Cat# FD0434
SCRI Renaissance 2200 Stain	Renaissance Chemicals	N/A
Sodium deoxycholate	Sigma-Aldrich	Cat# 30970
Solis Biodyne 5x HOT FIREPol EvaGreen qPCR Mix Plus	Solis Biodyne	Cat# 08-25-00001
Spectinomycin	Duchefa Biochemie	Cat# S0188
Toluidine blue O	Sigma-Aldrich	Cat# T3260
Urea	Sigma-Aldrich	Cat# U0631
Xylitol	Sigma-Aldrich	Cat# X3375
Critical commercial assays		
GeneJET GEL Extraction Kit	ThermoFisher	Cat# K0692
GeneJET Plant RNA purification kit	ThermoFisher	Cat# K0802
GeneJET Plasmid Miniprep Kit	ThermoFisher	Cat# K0503
Heat & Run gDNA removal kit	ArticZymes	SKU# 80200-50
Plant Ribo-Zero rRNA Removal Kit	Illumina	Cat# MRZSR116
TruSeq Stranded Total RNA HT Sample Prep Kit (with Ribo-Zero Plant)	Illumina	Cat# RS-122-2403
Deposited data		
RNA-seq data files	BioProject	PRJNA684618
Experimental models: Organisms/strains		
Arabidopsis: Col-0	Nottingham *Arabidopsis* Stock Centre	N/A
Arabidopsis: TCSn$_{pro}$:nYFP	Vatén et al.[18]	N/A

(*Continued on next page*)

Continued

REAGENT or RESOURCE	SOURCE	IDENTIFIER
Arabidopsis: TCSn$_{pro}$:erYFP	This manuscript	N/A
Arabidopsis: ARR5$_{pro}$:erYFP	Siligato et al.[36]	N/A
Arabidopsis: LBD1$_{pro}$:erYFP	This manuscript	N/A
Arabidopsis: LBD3pro:erYFP	This manuscript	N/A
Arabidopsis: LBD4$_{pro}$:erYFP	This manuscript	N/A
Arabidopsis: LBD11$_{pro}$:erYFP	This manuscript	N/A
Arabidopsis: ipt1;3;5;7	Miyawaki et al.[23]	N/A
Arabidopsis: arr1-3;arr10-5	Argyros et al.[37]	N/A
Arabidopsis: arr1-3;arr12-1	Argyros et al.[37]	N/A
Arabidopsis: lbd1c	This manuscript	N/A
Arabidopsis: lbd3c	This manuscript	N/A
Arabidopsis: lbd4c	This manuscript	N/A
Arabidopsis: lbd11c	This manuscript	N/A
Arabidopsis: lbd3c;lbd4c	This manuscript	N/A
Arabidopsis: lbd1c;lbd11c	This manuscript	N/A
Arabidopsis: lbd1c;lbd3c;lbd4c	This manuscript	N/A
Arabidopsis: lbd3c;lbd4c;lbd11c	This manuscript	N/A
Arabidopsis: lbd1c;lbd3c;lbd4c;lbd11c	This manuscript	N/A
Arabidopsis: tdr	Hirakawa et al.[24]	N/A
Arabidopsis: wox4	Hirakawa et al.[24]	N/A
Arabidopsis: tdr;wox4	Hirakawa et al.[24]	N/A
Arabidopsis: lbd3c;lbd4c;wox4	This manuscript	N/A
Arabidopsis: lbd3c;lbd4c;lbd11c;tdr	This manuscript	N/A
Arabidopsis: 35S:XVE>>cLBD1	This manuscript	N/A
Arabidopsis: 35S:XVE>>cLBD3	This manuscript	N/A
Arabidopsis: 35S:XVE>>cLBD4	This manuscript	N/A
Arabidopsis: 35S:XVE>>cLBD11	This manuscript	N/A
Arabidopsis: 35S:XVE>>CKX7-RFP	This manuscript	N/A
Arabidopsis: TCSn$_{pro}$:nYFP;35S:XVE>>CKX7-RFP	This manuscript	N/A
Arabidopsis: LBD3$_{pro}$:erYFP;35S:XVE>>CKX7-RFP	This manuscript	N/A
Arabidopsis: LBD4$_{pro}$:erYFP;35S:XVE>>CKX7-RFP	This manuscript	N/A
Arabidopsis: LBD3$_{pro}$:gLBD3-YFP;lbd3c;lbd4c	This manuscript	N/A
Arabidopsis: LBD4$_{pro}$:gLBD4-YFP;lbd3c;lbd4c	This manuscript	N/A
Arabidopsis: LBD11$_{pro}$:gLBD11-YFP;lbd1c;lbd3c;lbd4c;lbd11c	This manuscript	N/A
Arabidopsis: ARR5$_{pro}$:erYFP;35S:XVE>>cLBD3	This manuscript	N/A
Arabidopsis: TCSn$_{pro}$:nYFP;35S:XVE>>cLBD3	This manuscript	N/A
Oligonucleotides		
See Table S1	N/A	N/A
Recombinant DNA		
pDONRP41R	ThermoFisher	N/A
p1R4z-LBD1$_{pro}$	This manuscript	N/A
p1R4z-LBD3$_{pro}$	This manuscript	N/A

(*Continued on next page*)

Continued

REAGENT or RESOURCE	SOURCE	IDENTIFIER
p1R4z-LBD4$_{pro}$	This manuscript	N/A
p1R4z-LBD11$_{pro}$	This manuscript	N/A
p221z-erYFP	Siligato et al.[36]	N/A
p2R3a-nosT	Siligato et al.[36]	N/A
pBm43GW	Siligato et al.[36]	N/A
pHm43GW	Siligato et al.[36]	N/A
pDONR221	ThermoFisher	N/A
p1R4-35S:XVE	Siligato et al.[36]	N/A
p1R4z-TCSn$_{pro}$	This manuscript	N/A
pHm43GW-pTCSn:erYFP	This manuscript	N/A
p221z-cLBD1	This manuscript	N/A
p221z-cLBD11	This manuscript	N/A
pBm43GW-35S:XVE>>cLBD3	Zhang et al.[10]	N/A
pBm43GW-35S:XVE>>cLBD4	Zhang et al.[10]	N/A
pBm43GW-35S:XVE>>cLBD1	This manuscript	N/A
pBm43GW-35S:XVE>>cLBD11	This manuscript	N/A
p221z-CKX7	This manuscript	N/A
2R3z-tagRFP	Siligato et al.[36]	N/A
pCAM-kan-R4R3	Siligato et al.[36]	N/A
pCAM-kan-R4R3-35S:XVE>>CKX7-RFP	This manuscript	N/A
pHEE2E-TRI	Wang et al.[38]	N/A
2R3z-Bsa I-ccdB-Bsa I	Wang et al.[39]	N/A
p221z-zCas9- rbcS-E9t	This manuscript	N/A
p1R4- pEC1.2en EC1.1p	This manuscript	N/A
p2R3z-AtU3b-sgRNALBD1+AtU3d-sgRNALBD3+ AtU6-1-sgRNALBD4+AtU6-29-sgRNALBD4	This manuscript	N/A
pEC1.2en EC1.1p:zCas9- rbcS-E9t-*AtU3b-sgRNALBD1+AtU3d-sgRNALBD3+ AtU6-1-sgRNALBD4+AtU6-29-sgRNALBD4*	This manuscript	N/A
pHEE2E-TRI-LBD4	This manuscript	N/A
p221z-gLBD3	This manuscript	N/A
p221z-gLBD4	This manuscript	N/A
p221z-gLBD11	This manuscript	N/A
pBm43GW-LBD3$_{pro}$:gLBD3-YFP	This manuscript	N/A
pBm43GW-LBD4$_{pro}$:gLBD4-YFP	This manuscript	N/A
pBm43GW-LBD11$_{pro}$:gLBD11-YFP	This manuscript	N/A
Software and algorithms		
Chipster v3.11- v3.16	Kallio et al.[40]	https://chipster.csc.fi/; RRID: SCR_010939
Clustal X 2.1	Larkin et al.[41]	http://www.clustal.org/clustal2/; RRID: SCR_017055
clusterProfiler v3.16.1	Yu et al.[42]	http://bioconductor.org/packages/release/bioc/html/clusterProfiler.html; RRID: SCR_016884
CorelDRAW Graphics Suite 2020	CorelDRAW	http://www.coreldraw.com/en/product/graphic-design-software/; RRID: SCR_014235
dCAPs Finder v2.0	Neff et al.[43]	http://helix.wustl.edu/dcaps/
DESeq2	Love et al.[44]	https://bioconductor.org/packages/release/bioc/html/DESeq2.html; RRID: SCR_015687

(*Continued on next page*)

Continued

REAGENT or RESOURCE	SOURCE	IDENTIFIER
FastQC v0.11.3	Andrews[45]	https://www.bioinformatics.babraham.ac.uk/projects/fastqc/; RRID: SCR_014583
FIJI ImageJ v1.52	Schindelin et al.[46]	https://fiji.sc/; RRID: SCR_002285
ggplot2 v3.3.2	Wickham[47]	https://cran.r-project.org/web/packages/ggplot2/index.html; RRID: SCR_014601
gplots v3.1.0	Warnes et al.[48]	https://cran.r-project.org/web/packages/gplots/index.html
HTSeq	Anders et al.[49]	https://htseq.readthedocs.io/en/release_0.9.1/; RRID: SCR_005514
Leica Application Suite X	Leica Microsystems	https://www.leica-microsystems.com/products/microscope-software/p/leica-las-x-ls/; RRID: SCR_013673
Leica LAS AF Lite 2.6.x	Leica Microsystems	https://leica-las-af-lite.software.informer.com/2.6/
MEGA7	Kumar et al.[50]	https://megasoftware.net/; RRID: SCR_000667
R v4.0.2	The R Development Core Team[51]	https://www.r-project.org/
RStudio v1.4.1106	Racine[52]	https://www.rstudio.com/; RRID: SCR_000432
SPSS Statistics 26	IBM	https://www.ibm.com/products/spss-statistics; RRID: SCR_019096
TopHat2	Kim et al.[53]	http://ccb.jhu.edu/software/tophat/index.shtml; RRID: SCR_013035
Venny v2.1.0	Oliveros[54]	https://bioinfogp.cnb.csic.es/tools/venny/; RRID: SCR_016561
Other		
GENEWIZ	GENEWIZ	https://www.genewiz.com/
Bioanalyzer 2100	Agilent Technologies	https://www.agilent.com/cs/library/posters/Public/BioAnalyzer.PDF; RRID: SCR_019715
Leica DM2500 microscope	Leica Microsystems	https://www.leica-microsystems.com/products/light-microscopes/p/leica-dm2500/; RRID: SCR_020224
Leica M165 FC fluorescent stereo microscope	Leica Microsystems	https://www.leica-microsystems.com/products/stereo-microscopes-macroscopes/p/leica-m165-fc/
Leica Stellaris 8 confocal microscope	Leica Microsystems	https://www.leica-microsystems.com/products/confocal-microscopes/p/stellaris-8/
Leica TCS SP5 II confocal microscope	Leica Microsystems	https://downloads.leica-microsystems.com/Leica%20TCS%20SP5%20II/Brochures/Leica%20TCS_SP5_II-Brochure_Technical_Data.EN.pdf; RRID: SCR_018714
NanoDrop 1000 Spectrophotometer	ThermoFisher	http://tools.thermofisher.com/content/sfs/manuals/nd-1000-v3.8-users-manual-8%205x11.pdf; RRID: SCR_016517

RESOURCE AVAILABILITY

Lead contact

Further information and requests for resources and reagents should be directed to and will be fulfilled by Ari Pekka Mähönen (AriPekka.Mahonen@helsinki.fi).

Materials availability

Transgenic plant seeds and mutants generated in this study will be available on request.

Data and code availability

The RNA-seq data files are deposited under BioProject of NCBI (https://www.ncbi.nlm.nih.gov/bioproject) with accession number (BioProject ID: PRJNA684618).

EXPERIMENTAL MODEL AND SUBJECT DETAILS

All *Arabidopsis* lines used in this study were in *Col-0* background as detailed in the Key resources table. *Arabidopsis* seedlings were cultivated in a 22°C growth chamber under long day condition (16 h light and 8 h dark).

METHOD DETAILS

Plant material and growth conditions

Seeds were surface sterilized by sequentially incubating them in 20% chlorine and 70% ethanol for 1 min with vortexing, followed by washing twice in sterile water. The sterilized seeds were stratified in darkness at 4°C for two days. Seeds were plated on half-strength Germination Medium (½GM) containing 0.5x Murashige and Skoog salts,[35] 0.8% plant agar, 1% sucrose and 0,5g/l MES pH 5.8. The plates were placed vertically in a 22°C growth chamber with long day settings (16 h light and 8 h dark).

For cytokinin treatments, a 10 mM 6-benzylaminopurine (BAP, Sigma) stock solution dissolved in dimethyl sulfoxide (DMSO, Sigma) was prepared and a 1 μM working concentration was used. BAP or mock treatment was performed by transferring plants to ½GM plates supplied with an equal volume of BAP or DMSO and continuing growth for the indicated time. 17-β-oestradiol (17-β, Sigma) treatment was conducted in a similar way. The working concentration of 17-β for XVE-based gene induction was 5 μM unless stated otherwise. For cycloheximide treatment, 5-day-old plants were first immersed in liquid ½GM (without agar) supplemented with/without 50 μM cycloheximide (CHX) for 30 min with gentle shaking. BAP was added to a final concentration of 1 μM and plants were incubated for 1h. An equal volume of DMSO was used as a mock treatment.

The following transgenic lines and mutant alleles were published previously: *ipt1;3;5;7*[23], *ARR5*$_{pro}$*:erYFP*,[36] *TCSn*$_{pro}$*:nYFP*[18] (a modified version of Zürcher et al.[19]), *tdr*,[24]*wox4*,[24] *tdr;wox4*,[24] *arr1-3;arr10-5*[37] and *arr1-3;arr12-1*.[37]

Molecular cloning and transformation

LBD1 (AT1G07900), LBD4 (AT1G31320) and *LBD11 (AT2G28500)* promoters were cloned by amplifying a length of 3152 bp, 4434 bp and 4943 bp upstream of the transcription start site, respectively. A 2932 bp promoter sequence of *LBD3* (*AT1G16530*) was synthesized in GENEWIZ and the *TCS* promoter sequence was amplified from a published *TCSn*$_{pro}$*:nYFP* reporter line[18] (a modified version of Zürcher et al.[19]). All these promoter sequences were cloned into the *pDONRP41R* entry vector. The resulting entry vectors harboring different promoters, together with *p221z-erYFP*[36] and *p2R3a-nosT*,[36] were recombined into the destination vector *pBm43GW*[55] for LBDs or *pHm43GW*[55] for *TCS* by a MultiSite Gateway LR reaction. The coding sequence of *LBD1* and *LBD11* (with a stop codon) and the genomic sequence of *CKX7* (without a stop codon) were cloned into the *pDONR221* entry vector. The inducible overexpression constructs of *LBD1* and *LBD11* were generated by combining *p1R4-35S:XVE*,[36] *p221z-cLBD1/11* and *p2R3a-nosT*[36] with the destination vector *pBm43GW*.[55] The constructs *35S:XVE>>cLBD3* and *35S:XVE>>cLBD4* have been published before.[10] The inducible construct overexpressing *CKX7-tagRFP* fusion was made by integrating *p1R4-35S:XVE*,[36] *p221z-CKX7* and *p2R3z-tagRFP*[36] into *pCAM-kan-R4R3*.[36] All newly generated entry vectors were verified by Sanger sequencing and all binary constructs were transformed into *Col-0* ecotype by floral dipping.[56] Transgenic seedlings were screened (15-25 transgenic individuals per each construct) on selective ½GM plates supplied with 20 μg/ml DL-phosphinothricin (PPT, Duchefa Biochemie) *or* 20 μg/ml Hygromycin B Gold (InvivoGen). Homozygous single insertion lines were selected according to Mendelian segregation of a selection marker. For each construct, at least two transgenic lines with similar phenotype were identified for further analysis, and one was used as the representative in our analysis. The primers used in this study are listed in Table S1.

Mutant generation by CRISPR/Cas9

Since we did not find potential knock-out alleles for all four LBDs, we decided to generate new knock-out mutants for all of them by gene editing. The egg-cell specific promoter *pEC1.2en EC1.1p* and a codon optimized *zCas9* coding sequence with rbcS-E9t terminator were amplified from *pHEE2E-TRI*[38] and separately cloned into *pDONRP41R* and *pDONR221*. Four *sgRNA* expression cassettes targeting *LBD1*, *LBD3*, *LBD4* and *LBD11*, transcribed under promoters *AtU3b*, *AtU3d*, *AtU6-1* and *AtU6-29*,[57] respectively, were combined into *2R3z-Bsa I-ccdB-Bsa I*[39] by Golden Gate cloning as described previously.[39] All three entry vectors were assembled into *pBm43GW* by an LR reaction to make the *CRISPR/Cas9* binary construct.

The mutant screen was done in the T1 generation by sequencing PCR products of all four LBDs from 51 individual samples. T2 seeds were harvested from plants with heterozygous or homozygous mutations in the T1 generation for a construct-free mutant screen. To achieve this, seeds were geminated on ½GM plates containing 20 μg/ml PPT for 5 days, followed by transferal of PPT sensitive plants to PPT-free ½GM plates for another week to rescue them. The *LBD4* mutation was not obtained in T1 generation, likely because the *sgRNA* was driven by the *AtU6-1* promoter, which is less active in genome editing.[39] Therefore, another

independent *CRISPR/Cas9* construct targeting only *LBD4* was generated and transformed into the *lbd3c* background to make the *lbd3c;4c* double mutant. After segregating out the construct, the obtained *lbd3c;4c* knock-out mutant was crossed with the *lbd1c;11c* knock-out mutant, and the different mutant combinations used in this study were acquired in the F2 population. All *lbd* mutants used in this study contain frameshift mutations which give rise to a premature termination of translation and thus to truncated proteins. For clarity, elsewhere in this article *lbd1c*, *lbd3c*, *lbd4c* and *lbd11c* were written as *lbd1*, *lbd3*, *lbd4* and *lbd11*, respectively. More details can be found in Figure S2B.

To confirm that the observed phenotype was a consequence of the *CRISPR/Cas9* caused LBD mutation, a complementation assay was performed. We first cloned the genome sequence (without a stop codon) of *LBD3*, *LBD4* and *LBD11* into *pDONR221*. The resulting entry vectors *p221z-gLBD3/4/11* were recombined into the *pBm43GW*[55] destination vector together with entry vectors of the respective promoter and *p2R3a-YFP*[36] to generate the translational reporters $LBD3_{pro}$*:gLBD3-YFP,*$LBD4_{pro}$*:gLBD4-YFP* and $LBD11_{pro}$*:gLBD11-YFP,* respectively. Both $LBD3_{pro}$*:gLBD3-YFP and* $LBD4_{pro}$*:gLBD4-YFP* reporters complemented the *lbd3;lbd4* double mutant, and $LBD11_{pro}$*:gLBD11-YFP* reporter complemented the *lbd1;lbd3;lbd4;lbd11* quadruple mutant (Figures S2C–S2F).

Once the mutation type was determined, in the following cross experiments, we also performed dCAPs[43] (derived cleaved amplified polymorphic sequence, http://helix.wustl.edu/dcaps/) assays for genotyping analysis by digesting the PCR products of *LBD1*, *LBD3*, *LBD11* containing the target sites with *ScaI*, *DdeI* and *NotI*, respectively. The homozygous mutations identified by dCAPs were further confirmed by Sanger sequencing. The *LBD4* mutation was always genotyped by Sanger sequencing. All related primers are listed in Table S1.

Microscopy and image processing

To observe the anatomy of vascular tissue, plastic cross-sections were made from sections 5 mm below the root–hypocotyl junction unless otherwise stated. The sections were sequentially stained in 0.05% (w/v) toluidine blue solution and 0.05% (w/v) ruthenium red solution before imaging. The detailed sectioning methodology has been described before.[58] Plastic cross-section images were captured using a Leica 2500 microscope.

The live imaging of fluorescence reporters was conducted on a Leica M165 FC fluorescent stereo microscope equipped with the Leica Application Suite X package. In other cases, fluorescence observations were performed on a Leica TCS SP5 II and Stellaris 8 confocal microscopes. The samples were first fixed by incubating roots in 4% paraformaldehyde (dissolved in 1 × PBS, pH 7.2) for 1 h with vacuum, and then incubated at 4°C for several hours or overnight. Lateral view observations used fixed samples which were first washed twice in 1xPBS and then cleared with ClearSee solution[59] at room temperature for at least 1 day. Transverse observations used section cut with a vibratome as described elsewhere.[17] Cell walls were stained with 0.1% (v/v) SCRI Renaissance 2200 Stain. Confocal images were obtained with the Leica LAS AF Software.

To make the results comparable, microscopy settings were kept unchanged throughout each experiment. Heatmaps were generated using Leica AF Lite 2.6.x. Microsoft PowerPoint was used to crop and organize images. Images were sometimes rotated in CorelDRAW Graphics Suite 2020. The brightness of the fluorescence signal was sometimes manually adjusted for better visualization. In cases where images from mock and treatment were compared, the adjustments were always equal.

qRT-PCR

Total RNA was extracted with a GeneJET Plant RNA purification kit (ThermoFisher) according to the manufacturer's instructions and treated with DNase I (ThermoFisher). The cDNA was synthesized from 500 ng total RNA by using $Oligo(dT)_{18}$ primer (ThermoFisher) and the Maxima H Minus Reverse Transcriptase (ThermoFisher). Synthesized cDNA was diluted by adding equal volume of nuclease-free water. qPCR were performed in a 10 μL reaction volume consisting of 1 μL diluted cDNA, 2 μL 5 x EvaGreen qPCR mix (Solis Biodyne), 0.5 μL 5 μM forward and reverse primers and 6.5 μL nuclease-free water. qPCR was run on a Bio-Rad CFX384 cycler with following program: 95°C for 12 min, 45 cycles (95°C for 15 s, 60°C for 20 s, 72°C for 20 s). Amplification of target genes was analyzed by melting curve. Three biological repeats were conducted for each experiment and three technical repeats were included for each biological repeat. The relative expression levels were calculated by the $2^{-\Delta\Delta Ct}$ method[60] and normalized against three reference genes *UBQ10*, *ACT2* and *TIP41*. All qRT-PCR primers can be found in Table S1.

RNA-Seq

35S:XVE>>cLBD3 and *35S:XVE>>cLBD11* seeds were first germinated on ½GM plates for nine days, and then the 9-day-old seedlings were transferred to 5 μM 17-β induction or mock-plates for 8h or 24h. For each sample, root segments 0.5 cm-2 cm below the root-hypocotyl junction were collected from about 15 individuals. Visible lateral roots were removed. Three biological repeats were conducted for each time point. Total RNA was isolated using a GeneJET Plant RNA purification kit (ThermoFisher) following the manufacturer's instructions. RNA concentration and integrity were monitored using a NanoDrop 1000 Spectrophotometer (ThermoFisher) and a Bioanalyzer 2100 (Agilent Technologies). Genomic DNA and ribosomal RNA were removed using a Heat & Run gDNA removal kit (ArticZymes) and a Plant Ribo-Zero rRNA Removal Kit (Illumina), respectively. RNA-seq libraries were constructed using a TruSeq Stranded Total RNA Library prep kit (Illumina). The pooled samples were single-end sequenced on a NextSeq 500 sequencer with an HT 75 cycle kit v2.5 in 2 runs. Library construction and sequencing was done by the Sequencing and Genomics Laboratory, Institute of Biotechnology, University of Helsinki. Raw data can be accessed at BioProject of NCBI (https://www.ncbi.nlm.nih.gov/bioproject) with accession number (BioProject ID: PRJNA684618).

RNA-seq data analysis was performed using packages available in Chipster[40] (https://chipster.csc.fi/) and RStudio[52] (https://www.rstudio.com/) with the program R v4.0.2[51] (https://www.r-project.org/). FastQC[45] (https://www.bioinformatics.babraham.ac.uk/projects/fastqc/) was used to check the quality of the raw reads merged from 2 separate runs, and single-end reads (76 bp) were then mapped to the *Arabidopsis* reference genome (TAIR 10.36) using TopHat2[53] (http://ccb.jhu.edu/software/tophat/index.shtml). The reads aligning to exons of each gene were counted with HTSeq[49] (https://htseq.readthedocs.io/en/release_0.9.1/). Differential expression analysis between the mock and inductions was determined using the DESeq2 package[44] (https://bioconductor.org/packages/release/bioc/html/DESeq2.html). Subsequently, $|\log_2\text{FoldChange}| > 1$ and $p_{adjusted} < 0.05$ were applied to identify differentially expressed genes (DEGs). DEGs are listed in Data S1. For the hormone-related genes analysis in Table S2, the gene sets of *Arabidopsis* hormone synthetic pathway and signaling transduction were obtained from the Plant Hormone Research Network (RIKEN) database (http://hormones.psc.riken.jp/pathway_hormones.html) and Kyoto Encyclopedia of Genes and Genomes (KEGG) database[61] (https://www.genome.jp/kegg-bin/show_pathway?ath04075), respectively. Gene Ontology (GO) enrichment of biological processes in Data S3 and Figure S4 was performed using the clusterProfiler package[42] (http://bioconductor.org/packages/release/bioc/html/clusterProfiler.html) in R with $p < 0.05$. A Venn diagram (Figure S4C) was generated using Venny v2.1.0[54] (https://bioinfogp.cnb.csic.es/tools/venny/). The heatmap of A-type *ARR*s based on $\log_2$FC was done with the gplots[48] package in RStudio[52] (https://www.rstudio.com/) with the program R v4.0.2[51] (https://www.r-project.org/).

QUANTIFICATION AND STATISTICAL ANALYSIS

Cell file number, diameter and total area were measured manually in FIJI ImageJ v1.52.[46] The average cell area was calculated by dividing total area by cell file number. Plots were created with boxplot or the ggplot2[47] package in RStudio[52] (https://www.rstudio.com/) with the program R v4.0.2[51] (https://www.r-project.org/). Boxplots show the first quartile (lower limit of boxes), median (center line) and third quartile (upper limit of boxes). The red dots and empty circles in the boxplots represent individual samples and outliers, respectively. All experiments were repeated at least twice.

Statistical analyses were carried out using SPSS Statistics 26 and RStudio[52] (https://www.rstudio.com/) with the program R v4.0.2[51] (https://www.r-project.org/). Student's t test was used for comparing two groups. For multiple comparisons, one-way ANOVA analysis was done in SPSS Statistics 26. Levene's Test was used to test for homogeneity of variances. The significant differences between each dataset was calculated using a Tukey post hoc test (for equal homogeneous variance) or Tamhane's T2 test (for equal variance not assumed) at significance level alpha = 0.05. All ANOVA results can be found in Data S2.